BIOCHEMISTRY
including biophysical chemistry & molecular biology

Article

pubs.acs.org/biochemistry

NMR Localization of Divalent Cations at the Active Site of the *Neurospora* VS Ribozyme Provides Insights into RNA−Metal-Ion Interactions

Eric Bonneau and Pascale Legault*

Département de Biochimie et Médecine Moléculaire, Université de Montréal, C.P. 6128, Succursale Centre-Ville, Montréal, Québec H3C 3J7, Canada

Supporting Information

ABSTRACT: Metal cations represent key elements of RNA structure and function. In the *Neurospora* VS ribozyme, metal cations play diverse roles; they are important for substrate recognition, formation of the active site, and shifting the pK_a's of two key nucleobases that contribute to the general acid−base mechanism. Recently, we determined the NMR structure of the A730 loop of the VS ribozyme active site (SLVI) that contributes the general acid (A_{756}) in the enzymatic mechanism of the cleavage reaction. Our studies showed that magnesium (Mg^{2+}) ions are essential to stabilize the formation of the S-turn motif within the A730 loop that exposes the A_{756} nucleobase for catalysis. In this article, we extend these NMR investigations by precisely mapping the Mg^{2+}-ion binding sites using manganese-induced paramagnetic relaxation enhancement and cadmium-induced chemical-shift perturbation of phosphorothioate RNAs. These experiments identify five Mg^{2+}-ion binding sites within SLVI. Four Mg^{2+} ions in SLVI are associated with known RNA structural motifs, including the G−U wobble pair and the GNRA tetraloop, and our studies reveal novel insights about Mg^{2+} ion binding to these RNA motifs. Interestingly, one Mg^{2+} ion is specifically associated with the S-turn motif, confirming its structural role in the folding of the A730 loop. This Mg^{2+} ion is likely important for formation of the active site and may play an indirect role in catalysis.

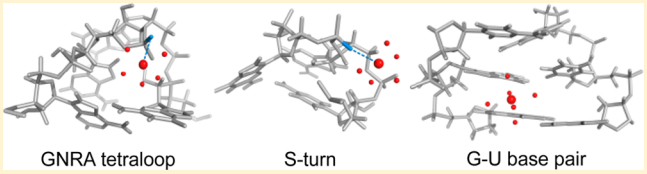

Metal cations play several essential functions in the biochemistry of RNA. Although Na^+, K^+, Mg^{2+}, and Ca^{2+} ions are the predominant cations in cells, Mg^{2+} is considered to be the most important in RNA folding.[1−4] Mg^{2+} can mediate helical packing,[5] promote long-range interactions,[2,6−9] organize multiway junction,[10] stabilize RNA motifs,[11−13] and reduce conformational fluctuations.[8,9,14] Mg^{2+} is particularly adept at stabilizing tightly packed phosphate oxygens found in several RNA conformations because of its small ionic radius, high charge density, and well-defined octahedral geometry that accommodates six inner-sphere ligands. In addition, Mg^{2+} can either form outer-sphere interactions with ligands through its first-hydration shell or specific inner-sphere interactions by displacing a water molecule and interacting directly with a ligand.

Following the discovery of the catalytic properties of ribozymes, the role of Mg^{2+} ions in catalysis has been intensively investigated. Mg^{2+} ions can play either a direct or an indirect role in the enzymatic mechanism.[3,15−17] Direct roles have been demonstrated including nucleophile activation,[18,19] coordination of nonbridging oxygens of the scissile phosphate,[20] promoting the optimal geometry of the reactive species,[21] and stabilization of the leaving group.[22] Potential indirect roles have been proposed involving long-range electrostatic stabilization[16] and/or alteration of pK_a's to facilitate a general acid−base mechanism.[16,23,24]

The *Neurospora* Varkud satellite (VS) ribozyme is a member of the small nucleolytic ribozyme family that also includes the hammerhead, hairpin, hepatitis delta virus (HDV), and *glms* ribozymes.[25−30] The VS ribozyme self-cleaves at the phosphodiester bond between G620 and A621 to generate products with 5′-OH and 2′−3′-cyclic phosphate termini. Its secondary structure contains six helical domains: the stem-loop I (SLI) contains the cleavage site and is considered as the substrate domain, whereas stem-loops II−VI (SLII−SLVI) form the catalytic domain (Figure 1A).[31] Substrate recognition is defined by a high-affinity kissing-loop interaction between the SLI and SLV terminal loops (Figure 1A) that induces a conformational change within the SLI substrate that is necessary for catalysis.[6,32−34] The proposed general acid−base mechanism involves the close association of the SLI and SLVI internal loops to form the active site,[35−39] where two nucleobases, G_{638} of SLI and A_{756} of the A730 loop, act as the general base and acid, respectively, in the cleavage reaction.[24,40−46] Although the secondary and tertiary structures of the VS ribozyme are unique among the nucleolytic ribozymes, its cleavage mechanism is similar to that of the hairpin ribozyme in which the active site is also formed by the

Received: October 31, 2013
Revised: December 19, 2013
Published: December 23, 2013

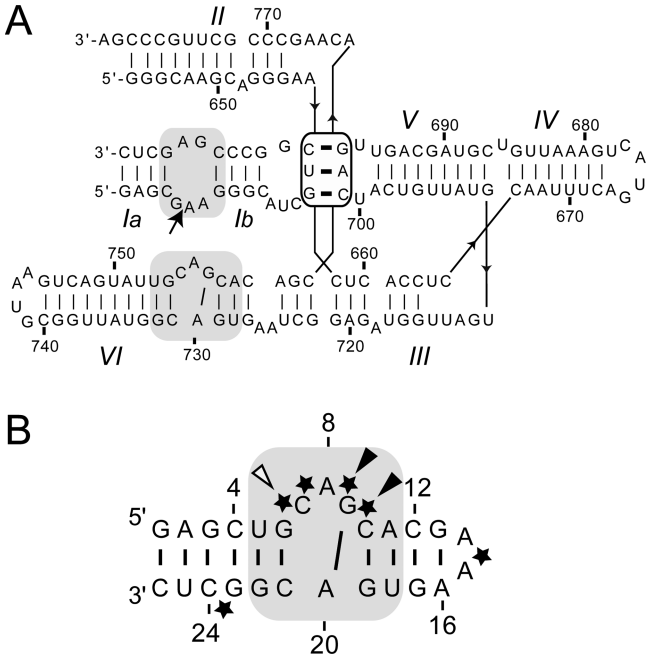

Figure 1. Primary and secondary structures of the *Neurospora* VS ribozyme and the SLVI RNA. (A) trans-Cleaving VS ribozyme (containing wild-type residues 648−777) with an SLI substrate. The cleavage site is shown by an arrow. Both the cleavage site internal loop and the active-site internal loop are shaded in gray, and the I/V kissing-loop interaction is boxed. (B) SLVI RNA, which includes the A730 loop of the VS ribozyme (gray shading). Phosphate groups that display inhibitory effects on cleavage when substituted by phosphorothioates are indicated by an arrow, and the arrow is filled for those cases where the activity can be rescued by addition of Mn^{2+} ions.[51] For this study, single phosphorothioate SLVI RNAs were prepared that contain either an S_p or R_p phosphorothioate at one of the phosphates indicated by black stars.

docking of two internal loops, and a nucleobase from each loop participates in the general acid−base mechanism.[30]

The VS ribozyme is dependent on the presence of divalent metal ions (Mg^{2+}, Mn^{2+}, or Ca^{2+}) or high concentration of monovalent salt for its cleavage activity.[47,48] Mg^{2+} ions have been found to be very important for several aspects of folding and function in the VS ribozyme. They are critical for substrate recognition, both for proper formation of the I/V kissing-loop interaction and for the conformational change in SLI.[6,31,35] In addition, they are required for folding of the two three-way junctions[49] and for formation of the active site.[35,37] Metal cations do not play a direct role in the general acid−base mechanism but appear to play an indirect role by altering the pK_a of the two key nucleobases.[24,50]

Phosphorothioate interference, chemical modifications, nucleotide analogue interference mapping, and NMR studies have been previously conducted in attempts to identify precisely the metal-binding sites in the VS ribozyme.[12,40,51−54] In the phosphorothioate interference-rescue experiments, the effect of *pro*-R_p phosphorothioate substitutions in the VS ribozyme were monitored on the Mg^{2+}-dependent cleavage, and several substitutions were shown to reduce the cleavage activity significantly.[51] Interestingly, the phosphorothioate inhibition of cleavage for select residues of the SLI loop (U_{631}), the SLV loop (C_{699}), and the A730 loop (G_{757} and C_{758}) could be rescued by thiophilic Mn^{2+} ions, suggesting that these phosphates are involved in inner-sphere metal coordination.[51]

Recently, we performed NMR studies with a small stem-loop containing the A730 internal loop, termed SLVI (Figure 1B), in order to gain structural insights into the formation of the VS ribozyme active site.[50] We established that Mg^{2+} ions are required to stabilize the structure of the A730 loop, and we determined the NMR structure of SLVI in the presence of Mg^{2+} ions. The NMR structure reveals a *cis*-WC/WC G−A base pair and an S-turn motif in the A730 loop that protrude the A_{756} into an enlarged minor groove such that it becomes available to participate in catalysis. Here, we extend these investigations by defining the precise locations of associated Mg^{2+} ions by combining Mn^{2+}-induced paramagnetic relaxation enhancement (PRE) with Cd^{2+}-induced chemical-shift perturbation (CSP) of phosphorothioate RNAs. These data are used to refine the NMR structure of SLVI to include five Mg^{2+}-ion binding sites. Four of the binding sites are associated with known RNA structural motifs, including the GNRA tetraloop and the G−U wobble pair. A comparison with similar structures from the PDB reveals new insights into the role of cation-binding sites in RNA structure. In agreement with the prior phosphorothioate interference-rescue experiments with the VS ribozyme,[51] one Mg^{2+} ion is associated with the S-turn motif, revealing its role in the folding of the A730 loop as well as a possible indirect role in catalysis.

EXPERIMENTAL PROCEDURES

Sample Preparation. Unlabeled, ^{15}N-labeled, and $^{13}C/^{15}N$-labeled SLVI RNAs (Figure 1B) were synthesized in vitro using T7 RNA polymerase (prepared in-house) and purified as described previously.[55] The SLVI RNAs containing phosphorothioate modifications at nonbridging phosphate oxygens (phosphorothioate RNAs; Figure 1B) were purchased as diastereomeric mixtures (Thermo Fisher Scientific, MA). These mixtures were first purified by denaturing polyacrylamide gel electrophoresis (20% acrylamide/bisacrylamide 19:1 and 7 M urea). The R_p and S_p isomers were subsequently separated by reverse-phase HPLC on a μBondapak C-18 column (10 μm and 7.8 × 300 mm; Waters, MA) using a multilinear gradient of HPLC-A (0.1 M ammonium acetate) and HPLC-B (0.1 M ammonium acetate and 50% acetonitrile) buffers at 1 mL/min: (a) 0−10% HPLC-B over 180 mL, (b) 10−13% HPLC-B over 120 mL, (c) 13−100% HPLC-B over 5 mL, and (d) 100−0% over 5 mL. The precise determination of configuration was made on the basis of enzymatic digestions with snake venom phosphodiesterase and Nuclease P1.[56]

The purified RNA samples were exchanged in NMR buffer A (10 mM sodium cacodylate, pH 6.5, 50 mM KCl, and 0.05 mM NaN_3 in 90% H_2O/10% D_2O) with Amicon Ultra-4 centrifugation filter devices (Millipore, MA). The RNAs were then heated at 95 °C for 2 min and then cooled in ice water for 5 min before changing to the final NMR buffer [NMR buffer A with either 5 mM $MgCl_2$ 99.995% (Sigma-Aldrich, MO) or a 5 mM mixture of varying concentrations of $MgCl_2$ 99.995% and $CdCl_2$ 99.999% (Sigma-Aldrich, MO)]. For NMR studies in D_2O, the samples were obtained by multiple cycles of lyophilization and resuspension in 99.996% D_2O.

NMR Spectroscopy. NMR experiments were conducted at either 15 or 25 °C on Varian ^{Unity}INOVA 500 and 600 MHz spectrometers equipped with a pulse-field gradient unit and an actively shielded z-gradient probe (either a $^1H/^{13}C/^{15}N$ triple resonance probe or a $^1H\{^{15}N-^{31}P\}$ indirect detection probe).

The NMR spectra were processed using the NMRPipe/NMRDraw package[57] and analyzed with NMRView.[58] ^{1}H, ^{13}C, and ^{15}N chemical shifts were referenced to an external standard of 2,2-dimethyl-2-silapentane-5-sulfonic acid (DSS)[59] at 0.00 ppm, and ^{31}P chemical shifts were referenced to an external standard of 85% phosphoric acid at 0.00 ppm.

Metal-Ion-Binding Studies. Manganese (Mn^{2+}) titrations were performed by adding small volumes of a concentrated solution (0.5 M) of 99.99% $MnCl_2$ (Sigma-Aldrich, MO) directly to the RNA sample to achieve final concentrations of 5, 10, 20, 40, and 80 μM $MnCl_2$. The first Mn^{2+} titration was carried out with a 0.9 mM $^{13}C/^{15}N$-labeled SLVI sample in NMR buffer A with 5 mM $MgCl_2$ and 100% D_2O. The paramagnetic effect was monitored by collecting 2D $^{1}H-^{13}C$ CT-HSQC[60,61] and 2D $^{1}H-^{13}C$ HMQC[62] spectra at 25 °C. A second Mn^{2+} titration was carried out with a 1.0 mM ^{15}N-labeled SLVI sample in NMR buffer A with 5 mM $MgCl_2$ and 90%:10% H_2O/D_2O. The paramagnetic effect was monitored by 1D ^{1}H watergate[63] and imino- and amino-optimized 2D $^{1}H-^{15}N$ HSQC[64] spectra at 15 °C. The third Mn^{2+} titration was carried out with a 1.0 mM ^{15}N-labeled SLVI sample in NMR buffer A with 5 mM $MgCl_2$ and 100% D_2O. The paramagnetic effect was monitored by 2D long-range $^{1}H-^{15}N$ HMQC[65] spectra at 25 °C optimized for detection of adenine N1/N3 atoms and purine N7/N9 atoms (J_{HN} = 21 Hz).

Cadmium (Cd^{2+}) titrations were conducted by exchanging the RNA samples with Amicon filters to NMR buffer A containing varying concentrations of $CdCl_2$ and $MgCl_2$. The total divalent-metal-ion concentration was kept constant at 5 mM under all conditions. A first Cd^{2+} titration was conducted with a 0.2 mM $^{13}C/^{15}N$-labeled SLVI RNA sample in 100% D_2O and $CdCl_2$ concentrations of 0.0625, 0.125, 0.25, 0.5, 1.0, 1.5, 2.5, and 4.0 mM. Chemical-shift changes (^{1}H and ^{13}C) were monitored for each $CdCl_2$ concentration from 2D $^{1}H-^{13}C$ CT-HSQC[60,61] spectra recorded at 25 °C. Additional Cd^{2+} titrations were conducted for SLVI RNAs with phosphorothioate modifications (0.15−0.4 mM) in 90%:10% H_2O/D_2O and $CdCl_2$ concentrations of 0.0625, 0.125, and 0.25 mM. Chemical-shift changes (^{1}H and ^{31}P) were monitored for each $CdCl_2$ concentration from 1D ^{1}H watergate[63] and 1D ^{31}P spectra recorded at 25 °C.

UV Spectroscopy and Determination of T_m Values. Thermal-stability studies of SLVI RNAs were conducted with a Cary 300 UV−vis spectrophotometer equipped with a Peltier temperature-control accessory. All samples contained 5 μM SLVI RNA in NMR buffer A supplemented with divalent metal ions (either 5 mM $MgCl_2$ or 4.75 mM $MgCl_2$/0.25 mM $CdCl_2$). Control samples were also prepared that contained only the selected buffers. Samples were heated from 25 to 98 °C at a rate of 1 °C/min, and absorbance data were collected at 260 nm after each 1 °C temperature increment. Subtraction of the control samples from the RNA samples was processed automatically using a dual-beam mode. Melting temperatures (T_m) were determined from the second derivative of the absorbance versus temperature curve, as previously described.[12] Reported T_m are averaged values derived from two or more individual UV-denaturation profiles.

Native Gel Electrophoresis. Nondenaturing polyacrylamide gel electrophoresis was carried out on 7.5% polyacrylamide gels, acrylamide/bisacrylamide (37.5:1) in Tris-borate buffer (50 mM Tris-borate, pH 8.0) supplemented with 20 mM magnesium acetate. The gels were prerun for 30 min at 200 V, loaded with RNA samples (2 μg of RNA at a concentration of 20 μM), and then run for 2 h at 250 V and 4 °C. The gels were stained with Stains All (Sigma-Aldrich, MO).

Structural Modeling of $Mg(H_2O)_n^{2+}$-Binding Sites. Three-dimensional structures of SLVI bound to $Mg(H_2O)_n^{2+}$ complexes were determined by complementing previously defined restraints[50] with distance restraints to position the five $Mg(H_2O)_n^{2+}$ complexes. These new restraints were derived from Mn^{2+}-induced paramagnetic relaxation enhancement (PRE) using the ratio of signal intensity (I_0/I_{Mn}) determined from 2D spectra collected at 0 μM $MnCl_2$ (I_0) and 10 μM $MnCl_2$ (I_{Mn}). For each signal in these spectra with $I_0/I_{Mn} \geq$ 8-fold and 4 $\leq I_0/I_{Mn} <$ 8-fold, distance restraints were set to 1.8−7.0 and 1.8−8.0 Å, respectively, between a defined Mg^{2+} center and the nuclei giving rise to the observed signal (Table S1 of Supporting Information). When the identity of the Mg^{2+} center could not be defined, ambiguous metal restraints were defined with bounds of 1.8−10.0 Å (Table S1 of Supporting Information). Restraints were also derived from Cd^{2+}-induced ^{31}P CSP of the sulfur-bound phosphorus from phosphorothioate SLVI RNAs [$\Delta_P = (\delta_{Mg} - \delta_{Cd})$] calculated from 1D ^{31}P spectra collected in 5 mM $MgCl_2$ (δ_{Mg}) and 0.25 mM $CdCl_2$/4.75 mM $MgCl_2$ (δ_{Cd}). Phosphorothioates with $\Delta_P \geq$ 1.0 ppm were considered as inner-sphere ligands, and a distance constraint of 1.8−2.2 Å was defined between a Mg^{2+} center and the modified nonbridging phosphate oxygen. Each phosphorothioate with 0.2 < Δ_P < 1.0 ppm was considered as an outer-sphere ligand, and a distance restraint of 1.8−7.0 Å was defined between a Mg^{2+} center and the modified nonbridging phosphate oxygen. On the basis of a clustering analysis of the nuclei that were most affected by Mn^{2+}-induced PRE ($I_0/I_{Mn} \geq$ 8-fold) and Cd^{2+}-induced CSP of phosphorothioates (Δ_P > 0.2 ppm), we inferred five distinct Mg^{2+}-binding sites for SLVI, termed sites 1−5, including two pentahydrated Mg^{2+}-ion complexes [$Mg(H_2O)_5^{2+}$; sites 1 and 3] and three fully hydrated Mg^{2+}-ion complexes [$Mg(H_2O)_6^{2+}$; sites 2, 4, and 5].

Three-dimensional structures of SLVI with bound $Mg(H_2O)_n^{2+}$ complexes were calculated by restraining molecular dynamics and simulated annealing with X-PLOR-NIH version 2.1.9[66] by adapting the two-stage protocol previously used for structure determination of free SLVI.[50] At stage one, an initial set of structures was calculated from RNA structures with randomized backbone angles to which $Mg(H_2O)_n^{2+}$ coordinates and parameters derived from HIC-Up were added.[67] Several rounds of calculations were performed at this stage to allow stepwise incorporation of restraints to metal-ion complexes. At the end of stage one, 50 structures were obtained that satisfy all distance and dihedral experimental restraints (no distance violation of >0.2 Å and no torsion angle violation of >5°), including all of those involving the five metal complexes. At stage two, these structures were refined with the same set of restraints but were supplemented with RDC restraints.[50] A final set of 500 structures was calculated, from which the 20 lowest-energy structures that satisfied the experimental restraints (no distance violation >0.2 Å, no torsion angle violation >5°, and no RDC violation >5 Hz) were selected for analysis. These 20 lowest-energy structures were used to calculate an average structure that was minimized against NOE and dihedral restraints. All structures were visualized and analyzed with PyMOL Molecular Graphics System, Version 1.3 Schrödinger, LLC.

Pattern Search of RNA Metal-Binding Motifs in the Protein Data Bank (PDB). Metal-binding motifs similar to those found in SLVI were searched in all available X-ray, cryo-

EM, and NMR structures of the PDB using WebFR3D.[68] The search patterns were defined according to their sequential and structural context in SLVI using the FR3D symbolic search algorithm. For each search, the results were extracted from the FR3D html file (raw hits) and filtered to remove the PDB files that did not contain metal ions. For each resulting hit (hit with a cation), a heavy-atom superposition of the nucleotides defining the search pattern was obtained between the PDB coordinates of the hit and the SLVI average structure, and this superposition was used to extract a pairwise heavy-atom rmsd. In cases where residues used for the superposition differ, the base of these residues was omitted for the superposition and rmsd calculation. The superposition was also used to extract the distance between the divalent metal ions of the two structures. For each FR3D search, those structures with metal distances smaller than 4.5 Å were termed positive hits and kept for further analysis.

RESULTS

Probing Divalent Metal-Ion-Binding Sites in SLVI through Mn^{2+}-Induced Paramagnetic Relaxation Enhancement (PRE). To identify metal-ion-binding sites in the SLVI RNA (Figure 1B), we performed several Mn^{2+} titrations and monitored them by NMR spectroscopy. Mn^{2+} is a paramagnetic metal ion that specifically enhances the relaxation of nuclei located within a short distance range (~10 Å).[69] The PRE is proportional to r^{-6} and can be used to derive distance (r) restraints between the Mn^{2+} and the observed nuclei.[69] Thus, Mn^{2+}-induced PRE represents a common approach for identifying divalent metal-ion-binding sites in RNA.[12,70−76]

Most of the previously assigned ^{1}H, ^{13}C, and ^{15}N signals in SLVI were probed using 2D $^{1}H-^{13}C$ and $^{1}H-^{15}N$ correlation experiments recorded during the titration of 0−80 μM $MnCl_2$ to an SLVI RNA folded in 5 mM $MgCl_2$. The high concentration of Mg^{2+} is necessary for proper RNA folding, whereas a ~1000-fold lower concentration of Mn^{2+} is sufficient for specific binding of the paramagnetic ion in the fast-exchange regime.[70,71,77] At 10 μM $MnCl_2$, the relaxation of several nuclei in SLVI is specifically affected, as shown for aromatic signals of the 2D $^{1}H-^{13}C$ CT-HSQC spectrum (Figure 2A,B) that either become significantly less intense (G_{13}) or completely disappear (G_1, G_3, G_6, G_9, C_{12}, G_{19}, G_{22}, and G_{23}). For each well-resolved signal in this and other 2D spectra, the signal intensity was measured in the absence (I_0) and presence of 10 μM Mn^{2+} (I_{Mn}) to calculate a disappearance ratio (I_0/I_{Mn}). Interestingly, the signals that undergo the strongest decrease in intensity ($I_0/I_{Mn} \geq 8$) correspond to ^{1}H, ^{13}C, and ^{15}N nuclei that are dispersed throughout the RNA (Figure 2C and Table S1 of the Supporting Information). Thus, the results from Mn^{2+}-induced PRE are compatible with several divalent-metal-binding sites in SLVI. The precise localization of these binding sites is, however, not possible at this stage because specific phosphates involved in metal binding could not be identified from Mn^{2+}-induced PRE as a result of the severe ^{31}P spectral overlap and the lack of specific ^{31}P assignment.

Identification of Phosphate−Metal Interactions by Cd^{2+}-Induced ^{31}P Chemical-Shift Perturbation (CSP) of Phosphorothioate RNAs. A phosphorothioate RNA contains a modification that substitutes either the *pro*-R_p or the *pro*-S_p nonbonded phosphate oxygen (*pro*-Rp/Sp OP) by a sulfur atom and significantly alters the chemical shift of the associated ^{31}P signal such that it can be easily identified in a 1D ^{31}P NMR spectrum.[78−80] Because phosphorothioates prefer thiophilic

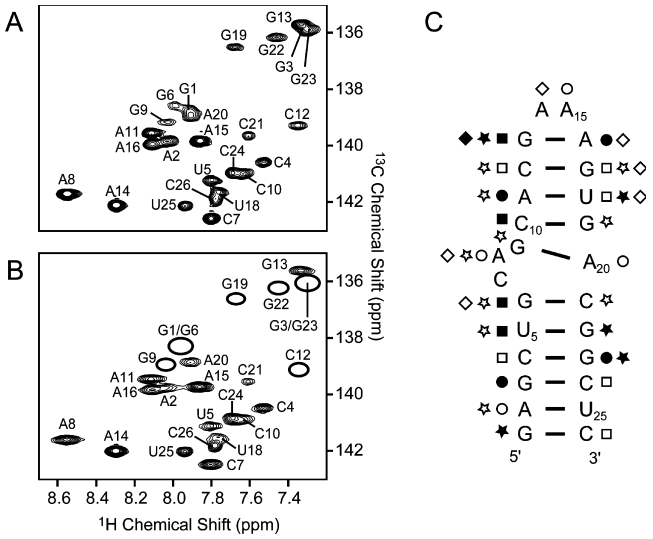

Figure 2. Probing divalent-metal-ion-binding sites in SLVI through Mn^{2+}-induced PRE. The effect of Mn^{2+} ions on the relaxation of SLVI nuclei is shown for aromatic (C6−H6 and C8−H8) signals by comparing the 2D $^{1}H-^{13}C$ HSQC spectra of SLVI RNA collected in (A) the absence and (B) the presence of 10 μM $MnCl_2$. Peaks that disappeared below the noise level are denoted with empty ovals. (C) Summary of the effect of Mn^{2+} ions on the relaxation of SLVI nuclei mapped on the secondary structure of SLVI. Filled and open symbols represent large ($I_0/I_{Mn} \geq$ 8-fold) and medium ($4 \leq I_0/I_{Mn} <$ 8-fold) PRE. Different symbols are used to distinguish PRE of imino and amino N−H signals (squares), N7, N9, and N3 signals (circles), aromatic C−H signals (stars), and ribose C−H signals (diamonds).

metal ions, like Cd^{2+}, over Mg^{2+} ions, formation of phosphorothioate−metal complexes can be monitored by recording 1D ^{31}P NMR spectra during Cd^{2+} titration.[79,80] Chemical-shift perturbations (CSP) of the sulfur-bound phosphorus have been associated with coordination of Cd^{2+} ions, with large upfield shifts being characteristic of inner-sphere coordination.[79,80]

To investigate the contribution of phosphates to metal coordination, several SLVI RNAs containing single phosphorothioate modifications were prepared (Figure 1B). Phosphorothioate modifications of C_7, A_8, G_9, and C_{10} are of particular interest to examine metal binding in the S-turn of SLVI. In addition, modification of A_{15} provides a positive control because an inner-sphere metal contact has been previously reported at this position of a GAAA tetraloop,[79] and modification of C_{24} provides a negative control because this residue is not predicted to interact with a metal ion. The phosphorothioate RNAs were prepared by chemical synthesis as mixtures of *pro*-R_p and *pro*-S_p isomers, and reverse-phase HPLC was used to separate the individual isomers. SLVI RNAs with a 5′-phosphorothioate at a specific residue N are denoted as either N-R_p or N-S_p. With the exception of the C24-R_p/S_p mixture, all of the individual isomers were separated from their mixtures in high purity.

The Cd^{2+}-titration conditions were carefully defined to prevent Cd^{2+}-induced structural changes in SLVI and/or RNA aggregation that may result from an excess of Cd^{2+} ions.[81,82] We first collected 2D $^{1}H-^{13}C$ CT-HSQC spectra of a 0.2 mM $^{13}C/^{15}N$-labeled SLVI RNA sample in the presence of increasing Cd^{2+} concentrations. Only small changes in chemical shifts were observed between 0 and 0.25 mM of Cd^{2+}, suggesting that the SLVI structure remains essentially intact.

dx.doi.org/10.1021/bi401484a | *Biochemistry* 2014, 53, 579−590

However, significant CSP are observed at Cd^{2+} concentrations ≥1.0 mM (Figure S1 of the Supporting Information), which indicates that the SLVI structure is significantly modified by high Cd^{2+}/RNA ratios. In addition, high Cd^{2+} concentrations cause smearing of SLVI on native gels (at 4 mM Cd^{2+}; not shown) and a change in the shape of the UV melting curves (at 1.5 mM Cd^{2+}; not shown), in agreement with aggregation of SLVI under these conditions.

To preserve the structural integrity of SLVI, Cd^{2+} titrations of phosphorothioate RNAs were thus performed at low Cd^{2+}/RNA ratios. These titrations were monitored by 1D ^{31}P spectra (Figure 3), and CSP of the sulfur-bound phosphorus was

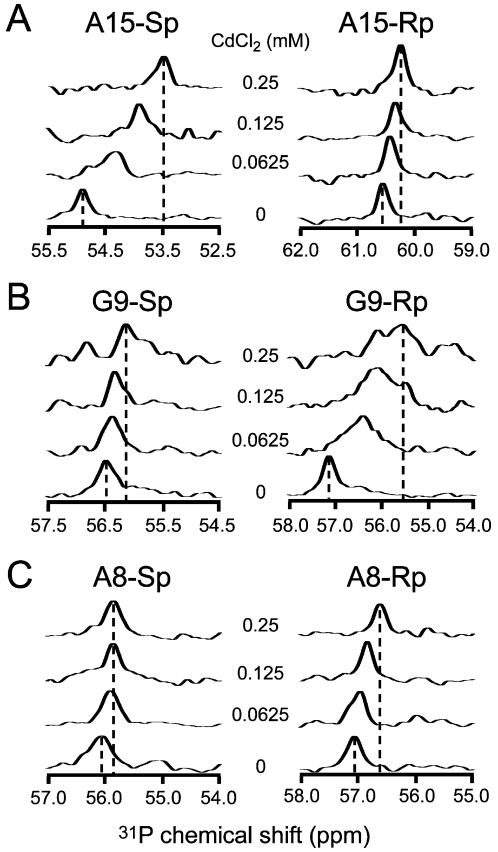

Figure 3. Effect of Cd^{2+} ions on the 1D ^{31}P NMR spectrum of selected SLVI RNAs containing single phosphorothioate modifications. The 1D ^{31}P spectra of (A) A15-S_p and A15-R_p, (B) G9-S_p and G9-R_p, and (C) A8-S_p and A8-R_p were collected in buffer containing $CdCl_2$/$MgCl_2$ concentrations of 0.0:5.0, 0.0625:4.9375, 0.125:4.875, and 0.25:4.75 mM. Only the most downfield region of the spectra containing the signal from the phosphorothioate is shown.

determined for each phosphorothioate RNA using $\Delta_P = (\delta_{Mg} - \delta_{Cd})$, where δ_{Mg} = chemical shift (δ) at 5 mM $MgCl_2$ and δ_{Cd} = δ at 4.75 mM $MgCl_2$/0.25 mM $CdCl_2$ (Table 1). A large CSP ($\Delta_P \geq 1.0$ ppm) was detected for the A15-S_p phosphorothioate (Δ_P = 1.43 ppm; Figure 3A and Table 1), as was previously observed for an equivalent phosphorothioate of a GAAA tetraloop involved in an inner-sphere metal coordination.[79] Similarly, the large CSP associated with the G9-R_p phosphorothioate (Δ_P = 1.62 ppm; Figure 3B and Table 1) provides evidence for inner-sphere metal coordination at the nonbridging G_9 *pro*-R_p phosphate oxygen. Smaller but still significant CSP ($0.2 < \Delta_P < 1.0$ ppm) for seven other phosphorothioates (C7-R_p/S_p, A8-R_p/S_p, G9-S_p, C10-R_p, and

Table 1. ^{31}P NMR CSP (Δ_P) Following Cd^{2+} Titrations of Phosphorothioate SLVI RNAs

phosphorothioate RNA	Δ_P (ppm)[a]
C7-R_p	0.31
C7−S_p	0.35
A8-R_p	0.41
A8-S_p	0.23
G9-R_p	1.62
G9-S_p	0.39
C10-R_p	0.32
C10−S_p	0.09
A15-R_p	0.35
A15-S_p	1.43
C24-R_p/S_p[b]	0.05/0.01

[a] $\Delta_P = (\delta_{Mg} - \delta_{Cd})$, where $\delta_{Mg} = \delta$ at 5 mM $MgCl_2$ and $\delta_{Cd} = \delta$ at 4.75 mM $MgCl_2$/0.25 mM $CdCl_2$. [b] This sample is a racemic mixture of R_p and S_p phosphorothioates.

A15-R_p; Figure 3, Figure S2 of the Supporting Information, and Table 1) are compatible with outer-sphere metal coordination. Finally, the C10-S_p and C24-R_p/S_p phosphorothioates display small CSP (Δ_P < 0.2 ppm; Figure S2 of the Supporting Information and Table 1), as is expected for those not involved in divalent metal coordination.

Previous reports have indicated that phosphorothioate modifications may affect RNA structure by inducing distortions in the sugar−phosphate backbone;[83,84] thus, control experiments were performed to verify that they have a minimal effect on the structure of SLVI. First, 1D ^{1}H imino NMR spectra were collected as part of the Cd^{2+} titration of phosphorothioate SLVI RNAs, and these spectra are all very similar to that of the unmodified SLVI (Figure S3 of the Supporting Information), suggesting that the phosphorothioate modifications do not significantly affect the global structure of SLVI. In addition, melting temperatures (T_m) were determined for each phosphorothioate RNA by UV−vis spectroscopy (Table 2). Generally, the observed T_m values of the phosphorothioate SLVI RNAs (Table 2) are very similar to that of the unmodified SLVI (74.6 ± 0.1 °C), further supporting that these modifications do not alter the structural integrity of the RNA.

Table 2. T_m Values for the Unmodified and Phosphorothioate SLVI RNAs

RNA	T_m (°C)
5 mM $MgCl_2$	
SLVI	74.6 ± 0.1
C7-R_p	64.6 ± 1.1
C7−S_p	74.4 ± 0.1
A8-R_p	74.3 ± 0.2
A8-S_p	74.5 ± 0.1
G9-R_p	74.2 ± 0.1
G9-S_p	73.8 ± 0.1
C10-R_p	73.7 ± 0.3
C10−S_p	73.4 ± 0.1
A15-R_p	82.5 ± 0.1
A15-S_p	75.0 ± 0.1
C24-R_p/S_p[a]	74.0 ± 0.2
4.75 mM $MgCl_2$ + 0.25 mM $CdCl_2$	
SLVI	74.6 ± 0.2
C7-R_p	73.5 ± 0.2

[a] This SLVI RNA is a racemic mixture of R_p and S_p phosphorothioates.

dx.doi.org/10.1021/bi401484a | *Biochemistry* 2014, 53, 579−590

However, significant differences in T_m values are noted for two phosphorothioate RNAs. The T_m value for the A15-R_p phosphorothioate (82.5 ± 0.1 °C) is 8 °C higher than that of the unmodified SLVI RNA, similar to what was previously observed for an equivalent residue in a GAAA hairpin loop.[83] In contrast, the T_m value for the C7-R_p phosphorothioate RNA (64.6 ± 1.1 °C) is 10 °C lower than that of the unmodified SLVI RNA, indicating that this particular modification destabilizes SLVI. Given the position of the C_7 5′-PO_4^- in the S-turn,[50] the destabilizing effect of the C7-R_p phosphorothioate modification could be due to a perturbed divalent metal coordination involving the modified atom. To investigate this possibility, T_m values were obtained in the presence of 0.25 mM Cd^{2+}/4.75 mM Mg^{2+} (Table 2). Interestingly, although this Cd^{2+}-containing buffer does not affect the stability of the unmodified SLVI RNA (T_m = 74.6 ± 0.2), it restores the stability of the C7-R_p phosphorothioate RNA (T_m = 73.5 ± 0.2), implying that the modified position is involved in metal coordination. Consequently, these controls support the validity of the Cd^{2+}-titration results, at least in terms of inferring specific phosphate−metal interactions in SLVI.

Structural Modeling of SLVI with $Mg(H_2O)_n^{2+}$ Complexes. Three-dimensional NMR structures of SLVI bound to $Mg(H_2O)_n^{2+}$ complexes ($SLVI^{Mg}$) were determined as previously reported for free SLVI ($SLVI^{free}$),[50] with the addition of Mg^{2+}-RNA distance restraints derived from the Mn^{2+}-induced PRE (Table S1 of the Supporting Information) and the Cd^{2+}-induced CSP of phosphorothioate RNAs (Table 1). Five $Mg(H_2O)_n^{2+}$ binding sites (sites 1−5) were defined by circumscribing into separate clusters atoms that were most affected by the Mn^{2+} and Cd^{2+} titrations. Metal complexes at sites 2, 4, and 5 were modeled as hexahydrated Mg^{2+} complexes [$Mg(H_2O)_6^{2+}$], whereas those at sites 1 and 3 were modeled as pentahydrated Mg^{2+} complexes [$Mg(H_2O)_5^{2+}$], given the evidence for inner-sphere metal coordination of the 5′-PO_4^- of A_{15} and G_9 (Table 1). The resulting 20 lowest-energy structures of $SLVI^{Mg}$ (Table 3) are compatible with all of the experimental restraints, indicating that the new Mg^{2+}−RNA restraints are fully consistent with distance, dihedral, and RDC restraints defined for structure determination of the $SLVI^{free}$ RNA.[50] The NMR structure of $SLVI^{Mg}$ is very well-defined with an overall heavy-atom rmsd of 0.33 ± 0.14 Å (Table 3). Thus, the ensemble of $SLVI^{Mg}$ structures is well-represented by the minimized average structure (Figure 4). By comparison, the NMR structure of $SLVI^{free}$ was previously determined with an overall heavy-atom rmsd of 0.67 ± 0.17 Å,[50] indicating that the new Mg^{2+}−RNA restraints help to define better the SLVI structure.

The structure of $SLVI^{Mg}$ reveals five well-defined Mg^{2+}-binding sites. The three outer-sphere metal-binding sites, sites 2, 4, and 5, are all located in the major groove of SLVI (Figure 5 and Table 4). Site 2 is located in the hairpin stem near the C_{10} 5′-PO_4^- of the S-turn (Figure 5A), where G_{17} O6, U_{18} O4, and G_{19} O6 act as potential outer-sphere ligands and C_{10} 5′-PO_4^- likely contributes to electrostatic stabilization. Site 4 is associated with the U_5−G_{22} wobble base within the 5′−3′ stem (Figure 5B), with U_5 O4, G_{22} O6/N7/5′-*pro*-R_p OP, and G_{23} O6/N7 acting as potential outer-sphere ligands and G_{22} 5′-PO_4^- ensuring electrostatic stabilization. Interestingly, the $Mg(H_2O)_6^{2+}$ complex at site 4 also interacts with the base of C_{21}, forming a cation−π interaction. The $Mg(H_2O)_6^{2+}$ complex at site 5 is found at the extremity of the 5′−3′ stem (Figure 5C), close enough to G_1 O5′/N7/O6, A_2 N7/5′-*pro*-R_p OP,

Table 3. Structural Statistics of the SLVI RNA with $Mg(H_2O)_n^{2+}$ Complexes

distance restraints	1086
number of NOE-derived distance restraints	965
internucleotide	591
intranucleotide	355
ambiguous	19
hydrogen-bond restraints	52
number of Mg^{2+}−RNA distance restraints	
from Mn^{2+}-induced PRE	60
from Cd^{2+}-induced CSP (Δ_p)	9
dihedral angle restraints	88
residual dipolar coupling restraints	30
total number of restraints	1204
rmsd from experimental restraints	
NOE (Å) (none >0.2)	0.0123 ± 0.004
dihedral (deg) (none >5°)	0.11 ± 0.01
residual dipolar couplings (none >5 Hz)	0.23 ± 0.01
rmsd from idealized geometry	
bonds (Å)	0.00547 ± 0.00002
angles (deg)	1.1741 ± 0.0007
impropers (deg)	0.441 ± 0.004
heavy-atom rmsd (Å)[a]	
overall (residues 2−25)	0.33 ± 0.14
5′−3′ stem (residues 2−5 and 22−25)	0.18 ± 0.08
hairpin stem (residues 11−18)	0.15 ± 0.07
A730 loop (residues 6−10 and 19−21)	0.23 ± 0.08
metal site 1 (residues 13−16)	0.087 ± 0.025
metal site 2 (residues 10−12 and 17−19)	0.14 ± 0.06
metal site 3 (residues 7−9)	0.23 ± 0.06
metal site 4 (residues 3−6 and 21−24)	0.20 ± 0.11
metal site 5 (residues 1−4 and 23−26)	0.17 ± 0.06

[a]Heavy-atom rmsd to the minimized averaged structure.

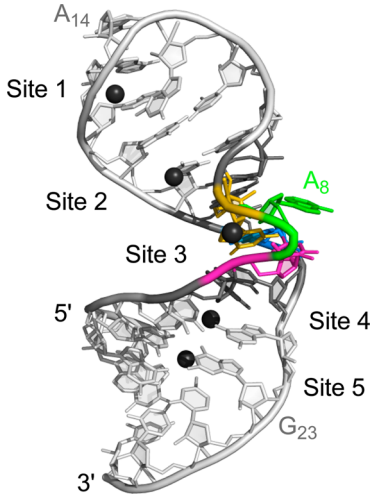

Figure 4. Lowest-energy structure of the SLVI RNA determined in the presence of $Mg(H_2O)_n^{2+}$ complexes. The five Mg^{2+} ions associated with SLVI are shown (black), but their bound water molecules were omitted for clarity. For SLVI, only the heavy atoms are shown, and the ribbon replacing the phosphorus and the nonbonded oxygen atoms is used to show the backbone. SLVI nucleotides are color-coded: the loop-closing base pairs (G_6-C_{21} and C_{10}-G_{19}) are dark gray, C_7 (C_{755}) is magenta, A_8 (A_{756}) is green, G_9 (G_{757}) is gold, and A_{20} (A_{730}) is blue.

dx.doi.org/10.1021/bi401484a | *Biochemistry* 2014, 53, 579−590

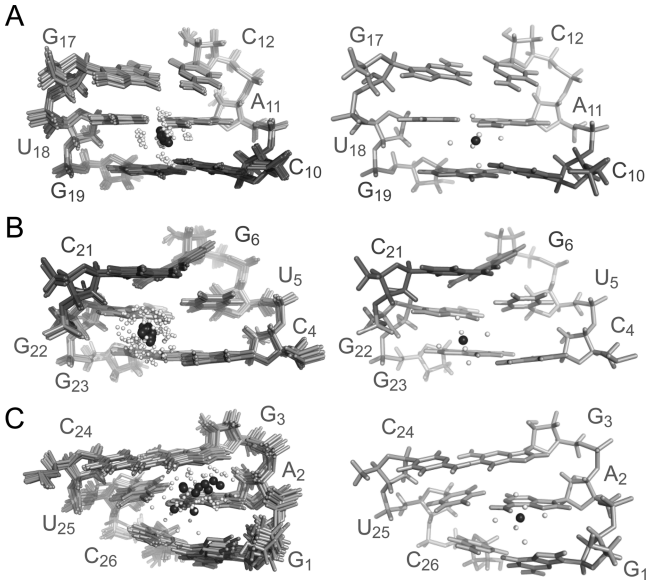

Figure 5. $Mg(H_2O)_6^{2+}$-binding sites associated with the (A) C_{10} 5′-PO_4^- (site 2), (B) G_{22}–U_5 wobble (site 4), and (C) 5′ end (site 5) of SLVI RNA. In panels A–C, a superposition of the 10 lowest-energy structures (left panel) and the lowest-energy structure (right panel) are shown. The Mg^{2+} ions are shown in black, with their bound water molecules in white.

and G_3 O6/N7 for outer-sphere coordination and to the 5′-PO_4^- of A_2 and G_3 for electrostatic stabilization. For site 5, the position of the $Mg(H_2O)_6^{2+}$ complex is not as well-defined as for sites 2 and 4 by the NMR data (Figure 5), indicating that metal coordination may be undergoing dynamic exchange of ligands.

The two inner-sphere metal-binding sites, sites 1 and 3 (Figure 6), are formed by unique structural elements within

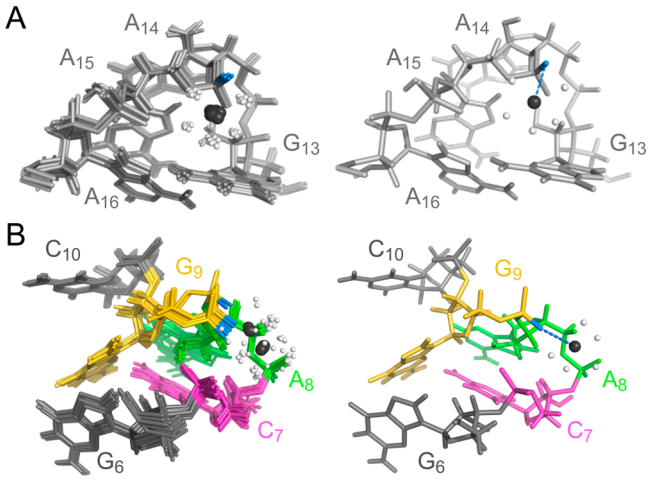

Figure 6. $Mg(H_2O)_5^{2+}$-binding sites associated with the (A) GAAA hairpin loop (site 1) and (B) S-turn (site 3) of SLVI RNA. In both panels A and B, a superposition of the 10 lowest-energy structures (left panel) and the lowest-energy structure (right panel) are shown. Blue dotted lines represent inner-sphere metal binding involving the A_{15} *pro*-S_p OP in panel A and the G_9 *pro*-R_p OP in panel B. The Mg^{2+} ions are shown in black, with their bound water molecules in white.

Table 4. Description of $Mg(H_2O)_n^{2+}$-Binding Sites in SLVI

site	inner-sphere ligands[a]	outer-sphere ligands[b]	electrostatic interactions[c]	cation–π interactions[d]
site 1 (n = 5)	A_{15} 5′-*pro*-S_p OP	A_{15} O5′	A_{15} 5′-PO_4^-	G_{13}
		A_{15} 5′-*pro*-R_p OP	A_{16} 5′-PO_4^-	
		A_{16} 5′-*pro*-R_p OP		
site 2 (n = 6)		G_{17} O6	C_{10} 5′-PO_4^-	
		U_{18} O4		
		G_{19} O6		
site 3 (n = 5)	G_9 5′- *pro*-R_p OP	C_7 O3′		
		C_7 O5′		
		C_7 5′-*pro*-R_p OP	C_7 5′-PO_4^-	
		A_8 O5′	A_8 5′-PO_4^-	
		A_8 5′-*pro*-R_p OP	G_9 5′-PO_4^-	
		G_9 O5′		
site 4 (n = 6)		U_5 O4	G_{22} 5′-PO_4^-	C_{21}
		G_{22} O6		
		G_{22} N7		
		G_{22} 5′-*pro*-R_p OP		
		G_{23} O6		
		G_{23} N7		
site 5 (n = 6)		G_1 O5′		
		G_1 N7		
		G_1 O6		
		A_2 N7	A_2 5′-PO_4^-	
		A_2 5′-*pro*-R_p OP	G_3 5′-PO_4^-	
		G_3 O6		
		G_3 N7		

[a]Inner-sphere ligands were determined from Cd^{2+}-induced CSP (Δ_P > 1.0 ppm). [b]Outer-sphere ligands were determined by selecting all hydrogen-bond acceptors within 4.0 Å of a $Mg(H_2O)_n^{2+}$ oxygen that were in a favorable orientation for outer-sphere interaction in at least 5 of the 20 lowest-energy structures. [c]Electrostatic interactions were determined by selecting 5′-PO_4^- within 8.0 Å of a Mg^{2+} ion. [d]Cation–π interactions were determined for Mg^{2+} ions within 5.2 Å and at an angle smaller than 52° from the ring centroid.[85]

dx.doi.org/10.1021/bi401484a | *Biochemistry* 2014, 53, 579–590

SLVI that contain electronegative pockets rich in phosphate oxygens, with one of the phosphates involved in inner-sphere metal coordination (A_{15} 5′-*pro*-S_p OP at site 1 and G_9 5′-*pro*-R_p OP at site 3; Table 4). Site 1 within the $G_{13}A_{14}A_{15}A_{16}$ tetraloop also utilizes three potential outer-sphere ligands identified as A_{15} O5′/5′-*pro*-R_p OP and A_{16} 5′-*pro*-R_p OP (Table 4). Remarkably, the $Mg(H_2O)_5^{2+}$ at site 1 is positioned on one face of the G_{13} base, forming a cation−π interaction (Figure 6A).[85] Site 3 also involves several potential outer-sphere ligands identified as C_7 O3′/O5′/5′-*pro*-R_p OP, A_8 O5′/5′-*pro*-R_p OP, and G_9 O5′ (Table 4). Moreover, site 3 is unique in that the 5′-PO_4^- of C_7, A_8, and G_9 within the S-turn form an electronegative cluster resembling a three-prong mount that holds the $Mg(H_2O)_5^{2+}$ complex (Figure 6B).

Search for Metal-Binding Motifs in the PDB. To complement our NMR study of metal-binding sites in SLVI, we used the WebFR3D symbolic search algorithm[68] to find similar metal-binding sites in the PDB. The search patterns correspond to sites 1−5 (Figure 4), as summarized in Table S2 of the Supporting Information. Positive hits from this search fit the search pattern and also contain a metal ion that is within 4.5 Å of that found for the same motif in SLVI.

For the GNRA motif in SLVI (site 1), the search pattern was defined by the consecutive CGNRAG sequence (N is an undefined nucleotide and R is a purine), with the first and last nucleotides forming a Watson−Crick base pair. The search resulted in three positive hits with pairwise heavy-atom rmsd values and metal distances to the SLVI average structure of 1.0−1.3 and 0.7−4.1 Å, respectively (Figure 7A). All of these

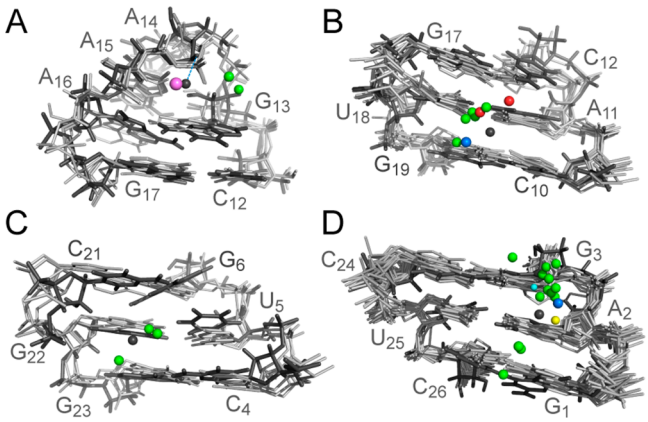

Figure 7. Superposition of metal-binding sites in SLVI with PDB structures containing similar metal-binding sites identified using WebFR3D. The metal-binding sites in SLVI are associated with the (A) GNRA hairpin loop (site 1), (B) C_{10} 5′-PO_4^- (site 2), (C) G_{22}−U_5 wobble (site 4), and (D) 5′ end (site 5). The structure and Mg^{2+} ions of SLVI are shown in black, whereas the other structures (PDB entries in Table S2 of Supporting Information) are shown in gray, with their associated metal ion color coded according to the type of metal (Mg^{2+}, green; Na^+, purple; Co^{3+}, red; Ca^{2+}, blue; Ni^{2+}, yellow; and Ir^{3+}; light blue).

motifs adopt a GNRA tetraloop fold with a metal ion in the minor groove interacting with the 5′-PO_4^- corresponding to that of A_{15} in SLVI, although this interaction does not involve inner-sphere coordination as observed for SLVI. Remarkably, in all cases, the metal ion forms a cation−π interaction with the conserved G nucleobase of the motif.

For site 2, the search pattern corresponds to a 3 bp helical domain that matches the exact sequence of the first three base pairs of the hairpin stem (C_{10}-C_{12}/G_{17}-G_{19}). The search resulted in eight positive hits, with pairwise heavy-atom rmsd values and metal distances to the SLVI average structure of 0.6−1.1 and 1.6−3.4 Å, respectively (Figure 7B). From the superposition of the eight positive hits to the average SLVI structure, it is clear that the associated metal ions always lie in the major groove, although they occupy several different locations within this ensemble of structures.

For the S-turn motif (site 3), two search patterns were defined from the A730 loop sequence (Table S2 of the Supporting Information); however, only one raw hit (i.e., without metal) was obtained corresponding to the previously determined SLVI structure.[50]

For the G−U base pair in SLVI (site 4), the search pattern was defined as a helical domain with three Watson−Crick base pairs corresponding to nucleotides C_4-G_6/C_{21}-G_{23} in SLVI. This search resulted in three positive hits with pairwise heavy-atom rmsd values and metal distances to the SLVI average structure of 1.0−1.9 and 1.5−2.0 Å, respectively (Figure 7C). In one case (PDB code 1FJG), the divalent metal ion forms a cation−π interaction with a cytidine.[85]

For the purine stretch at the 5′ end of the helix (site 5), the search pattern corresponds to a 3 bp helical domain that matches the exact sequence of the three first base pairs in SLVI (G_1-G_3/C_{24}-C_{26}). The search resulted in 16 positive hits with pairwise heavy-atom rmsd values and metal distances to the SLVI average structure of 0.4−1.1 and 1.7−4.0 Å, respectively (Figure 7D). From the superposition of the 16 positive hits to the average SLVI structure, it is clear that the associated metal ions lie in the major groove, although they occupy a variety of different locations in these structures.

DISCUSSION

Powerful NMR Approach for Localization of Divalent Metal-Binding Sites in RNA. The present work highlights the strength of combining Mn^{2+}-induced PRE experiments and Cd^{2+}-induced CSP of phosphorothioate RNAs to localize divalent-cation-binding sites in RNA. Mn^{2+}-induced PRE experiments have been widely used to probe RNA structures and to define metal-binding sites[9,12,71,74,76] and can provide a large number of RNA−metal restraints, especially for ^1H, ^{13}C, and ^{15}N atoms of $^{13}C/^{15}N$-labeled RNAs. However, Cd^{2+}-induced CSP of phosphorothioate RNAs identifies specific metal−phosphate interactions and provides information on the coordination state of the associated metal ions.[79,80,86−88] Thus, these two approaches are complementary, and together they provide a large number of nonredundant experimental restraints to define precisely metal-ion binding in the SLVI RNA. An important consideration in using this dual approach is ensuring that the different metal ions and chemically modified RNAs employed do not affect the structural integrity of the RNA. Importantly, the two metal ions used, Mn^{2+} and Cd^{2+}, both support the catalytic activity of the VS ribozyme and thus likely the correct folding at the active site.[47,48,51] In addition, experimental controls were performed to ensure reliable measurement of distance restraints between the RNA and the associated divalent metals. Overall, the distance restraints derived from these data help to define better the structure of SLVI and to allow the localization of five well-defined divalent metal-binding sites in the major groove of the RNA. One of the metal-binding sites is specific to the S-turn of the A730 loop of SLVI, whereas the other four are commonly found in other RNAs. Thus, the NMR structure of SLVI with bound divalent

cations provides valuable insights into both our general understanding of RNA−metal interactions and the cation requirement for formation of the VS ribozyme active site.

New Insights about Known Cation-Binding Sites in RNA. According to our FR3D search, four of the five metal-binding sites in SLVI have been previously observed in similar RNA structures. Two of these sites (sites 2 and 5) bind a hexahydrated Mg^{2+} ion within the major groove of A-form helical stems formed by standard Watson−Crick base pairs. The site located at the 5′ end of SLVI (site 5) is formed by three consecutives purines. This site offers a favorable environment for cations because of the presence of several electronegative groups associated with the 5′-GAG-3′ sequence. This metal-binding site is not as well-defined by the NMR data as other sites in SLVI, suggesting that more than one coordination mode are possible and that diffuse binding may occur along the purine stretch. Using FR3D, we identified 16 similar metal-binding sites in purine patches with the same sequence and structure context. The location of the metal is also not well-defined within these metal-binding sites, further supporting that the major groove of consecutive purines represents a common metal-binding site in double-stranded RNA that allows diffuse binding over the Hoogsteen edge of these purines.[71,74,89] In contrast, the binding of a Mg^{2+} ion within the hairpin stem at site 2 is better defined, with the base keto-oxygens of the 5′-GUG-3′ sequence and the *pro*-R_p OP of the C_{10} 5′-PO_4^- as potential outer-sphere ligands. Using FR3D, we identified eight similar sites in the PDB, and the location of the metal ion is more clearly defined within these available structures than for the 5′-GAG-3′ site, indicating fewer modes of metal coordination at the 5′-GUG-3′ site. These results also point out sequence-dependent variations in cation binding within the major groove of A-form RNA helices.

G−U wobble pairs are well-known metal-binding sites that form depending on the sequence and structure context.[5,71,73,90−93] In SLVI, a metal ion is associated with the G_{22}−U_5 base pair in the 5′−3′ stem near the A730 loop (site 4). The Hoogsteen edges of G_{22} and G_{23} are mainly involved in the interaction with the hexahydrated Mg^{2+} ion, in agreement with previous studies. In the structure of SLVI, a cation−π interaction is also observed between the Mg^{2+} ion and the C_{21} nucleobase.[85] To our knowledge, this interaction has not been previously associated with a G−U wobble pair. Using FR3D, we found three similar structures in the PDB. Interestingly, in one of these three structures (PDB entry 1FJG),[94] the bound metal ion also forms a cation−π interaction with a cytidine. In this case, however, the metal ion is located further from the center of the base and has a larger angle with the centroid of the nucleobase, suggesting a weaker cation−π interaction. In SLVI, the nearby A730 loop may render C_{21} more accessible for a cation−π interaction with the Mg^{2+} ion. However, given that the G−U pair is found in a different context in SLVI versus the full-length VS ribozyme, it is not clear if Mg^{2+} binding at this site is relevant to the activity of the ribozyme.

The GNRA tetraloop has been extensively characterized as a metal-binding site.[72,79,95−97] In the context of the present study, the GAAA loop of SLVI was used as a positive control because an inner-sphere divalent-metal interaction involving the 5′-PO_4^- of A_{15} was previously identified in an equivalent position of a GAAA hairpin on the basis of Cd^{2+} titration of phosphorothioates.[79] These NMR results were essentially reproduced here for the GNRA loop of SLVI. In addition, we identified a cation−π interaction in the SLVI structure between the Mg^{2+} ion and the pyrimidine ring of the first G nucleobase of the GNRA loop. The importance of this cation−π interaction in the GNRA fold has not been previously established, at least to our knowledge; therefore, it is interesting to examine cation binding to other GNRA loop structures in the PDB. Using FR3D, we identified three other similar GNRA loop structures associated with a cation. Remarkably, although the precise location of the cation differs between these structures, it always interacts with the R 5′-PO_4^- and forms a cation−π interaction with the conserved G nucleobase.

Cation-Binding Site in the A730 Loop Is Important for the Activity of the VS Ribozyme. From previous NMR studies, we established that the presence of Mg^{2+} ions is required for the formation of a stable A730 loop. It is now clear that binding of a specific Mg^{2+} ion at the S-turn (site 3) is central to the folding of the A730 loop.[50] This S-turn brings three phosphate groups in proximity to one another [5′-PO_4^- of C_7 (C_{755}), A_8 (A_{756}), and G_9 (G_{757})] with particularly short OP−OP distances between G_9 and C_7 and between G_9 and A_8 (4.1 and 5.1 Å, respectively, in the average structure). This tight packing of repulsive electronegative charges is dependent on the multidentate chelation of a Mg^{2+} ion, which involves an inner-shell ligand [5′-*pro*-R_p OP of G_9 (G_{757})] and several potential outer-sphere ligands. Although our FR3D search indicates that there is no precedent for a S-turn structure in a similar loop context, the S-turn motif is found in other structural contexts, both with or without a divalent cation.[74,98−102] With the A730 loop being relatively small, this clearly imposes topological and electrostatic constraints on the phosphate backbone at the S-turn that prevents stable folding in the absence of metal ions.

In previous work with the VS ribozyme, phosphorothioate interference and manganese-rescue experiments suggested that the *pro*-R_p OP of G_{757} (G_9) and C_{758} (C_{10}) are involved in direct metal binding and that the phosphate group of C_{755} (C_7) makes an outer-sphere contact to a metal ion or participates in hydrogen bonding.[40,51] The NMR studies of SLVI reveal an outer-sphere metal contact for C_{755} (C_7) *pro*-R_p OP and an inner-sphere metal contact for G_{757} (G_9) *pro*-R_p OP, in agreement with the biochemical studies.[51] For C_{758} (C_{10}), the NMR studies reveal an outer-sphere contact to a Mg^{2+} ion but not the predicted inner-sphere contact.[51] Within SLVI, the C_{758} 5′-PO_4^- may partially contribute to stabilization of the S-turn via an outer-sphere interaction with a Mg^{2+} ion in the hairpin stem. However, within the context of the VS ribozyme, this metal interaction may be modified because of nearby elements of secondary and tertiary structures, including formation of the active site between stem-loops I and VI. In summary, our NMR studies of SLVI generally agree with phosphorothioate interference of VS ribozyme cleavage, which indicates that the Mg^{2+}-dependent S-turn in the A730 loop is essential for catalysis by the VS ribozyme.[50]

The Mg^{2+} ion at the S-turn plays a structural role in catalysis by the VS ribozyme by allowing the folding of the S-turn in the A730 loop and enabling A_{756} to be extruded in the minor groove to participate as a general acid in catalysis.[50] In the hairpin ribozyme, which catalyzes phosphodiester-bond cleavage by a similar mechanism,[30] the proposed general acid in the reaction (A_{38}) also protrudes from an S-turn structure that is stabilized by at least two divalent cations.[103,104] Although these cations do not play a direct role in the cleavage mechanism, they may contribute either through electrostatic stabilization or by modulating the pK_a of functional residues.[16,23] In the VS

dx.doi.org/10.1021/bi401484a | *Biochemistry* 2014, 53, 579−590

ribozyme, it is also unlikely that the Mg^{2+} ion at the S-turn plays a direct role in catalysis, given that its binding site is remote from the scissile phosphate in a model of the VS ribozyme active site.[50] Nevertheless, given that this Mg^{2+} ion is not too distant from the catalytic site, we can not rule out the possibility that it contributes to the chemistry of the reaction. It is known that the pK_a value of the A_{756} and the G_{638} nucleobases are shifted toward neutrality to facilitate the cleavage reaction[40,41,43−46] and that the pK_a of these nucleobases is modulated by the identity of the metal cation.[24] Thus, the Mg^{2+} ion in the A730 loop clearly plays a structural role in defining the VS ribozyme active site, but it also likely contributes indirectly to the general acid−base chemistry.

■ ASSOCIATED CONTENT

Supporting Information

Effect of Cd^{2+} on the 2D $^{1}H-^{13}C$ HSQC spectrum of SLVI RNA; effect of Cd^{2+} on the 1D ^{31}P NMR spectrum and ^{1}H imino NMR spectrum of SLVI RNAs containing a single phosphorothioate modification; distance restraints derived from Mn^{2+}-induced PRE; and results from the WebFR3D motif search. This material is available free of charge via the Internet at http://pubs.acs.org.

Accession Codes

The NMR chemical shifts, structural restraints, and structural coordinates of SLVI with bound $Mg(H_2O)_n^{2+}$ complexes have been deposited through the RCSB Protein Data Bank and given BMRB entry code 19692 and PDB entry code 2MIS.

■ AUTHOR INFORMATION

Corresponding Author

*E-mail: pascale.legault@umontreal.ca. Phone: 514-343-7326.

Funding

This work was supported by a Canadian Institutes of Health Research (CIHR) grant (MOP-86502) as well as graduate scholarships (E.B.) from CIHR and the Université de Montréal. P. L. holds a Canada Research Chair in Structural Biology and Engineering of RNA.

Notes

The authors declare no competing financial interest.

■ ACKNOWLEDGMENTS

We are very grateful to Luke Ward and Victoria De Rose for useful discussions and to Nicolas Girard for help with motif search in WebFR3D. We also thank Patricia Bouchard and James G. Omichinski for their critical reading of the manuscript.

■ ABBREVIATIONS USED

2D, two dimensional; 3D, three dimensional; bp, base pair; Cd^{2+}, cadmium; CSP, chemical-shift perturbation; CT, constant time; δ, chemical shift; Δ_P, ^{31}P CSP of the phosphorothioate; HSQC, heteronuclear single quantum coherence; Mg^{2+}, magnesium; Mn^{2+}, manganese; NOE, nuclear Overhauser effect; NOESY, NOE spectroscopy; OP, phosphate oxygen; PO_4^-, phosphate; PRE, paramagnetic relaxation enhancement; PDB, protein data bank; rmsd, root-mean-square deviation; T_m, melting temperature

■ REFERENCES

(1) Feig, A. L., and Uhlenbeck, O. C. (1999) The role of metal ions in RNA biochemistry, In *The RNA World* (Gesteland, R. F., Cech, T. R., and Atkins, J. F., Eds.) 2nd ed., Cold Spring Harbor Laboratory Press, New York.

(2) Hsiao, C., Tannenbaum, E., VanDeusen, H., Herkshkovitz, E., Perng, G., Tannenbaum, A. R., and Williams, L. D. (2009) Complexes of nucleic acids with group I and II cations, In *Nucleic Acid-Metal Ion Interactions* (Hud, N. V., Ed.) RSC Publishing, Cambridge, UK.

(3) Frederiksen, J. K., Fong, R., and Piccirilli, J. A. (2009) Metal ions in RNA catalysis, In *Nucleic Acid-Metal Ion Interactions* (Hud, N. V., Ed.) RSC Publishing, Cambridge, UK.

(4) DeRose, V. J. (2009) Characterization of nucleic-acid-metal ion binding by spectroscopic techniques, In *Nucleic Acid-Metal Ion Interactions* (Hud, N. V., Ed.) p 447, RSC Publishing, Cambridge, UK.

(5) Cate, J. H., and Doudna, J. A. (1996) Metal-binding sites in the major groove of a large ribozyme domain. *Structure 4*, 1221−1229.

(6) Rastogi, T., Beattie, T. L., Olive, J. E., and Collins, R. A. (1996) A long-range pseudoknot is required for activity of the *Neurospora* VS ribozyme. *EMBO J. 15*, 2820−2825.

(7) Klein, D. J., Moore, P. B., and Steitz, T. A. (2004) The contribution of metal ions to the structural stability of the large ribosomal subunit. *RNA 10*, 1366−1379.

(8) Selmer, M., Dunham, C. M., Murphy, F. V. t., Weixlbaumer, A., Petry, S., Kelley, A. C., Weir, J. R., and Ramakrishnan, V. (2006) Structure of the 70S ribosome complexed with mRNA and tRNA. *Science 313*, 1935−1942.

(9) Noeske, J., Schwalbe, H., and Wohnert, J. (2007) Metal-ion binding and metal-ion induced folding of the adenine-sensing riboswitch aptamer domain. *Nucleic Acids Res. 35*, 5262−5273.

(10) Lilley, D. M. (2000) Structures of helical junctions in nucleic acids. *Q. Rev. Biophys. 33*, 109−159.

(11) Cabello-Villegas, J., Tworowska, I., and Nikonowicz, E. P. (2004) Metal ion stabilization of the U-turn of the A_{37} N^6-dimethylallyl-modified anticodon stem-loop of *Escherichia coli* $tRNA^{Phe}$. *Biochemistry 43*, 55−66.

(12) Campbell, D. O., Bouchard, P., Desjardins, G., and Legault, P. (2006) NMR structure of Varkud satellite ribozyme stem-loop V in the presence of magnesium ions and localization of metal-binding sites. *Biochemistry 45*, 10591−10605.

(13) Lilley, D. M. (2012) The structure and folding of kink turns in RNA. *WIREs RNA 3*, 797−805.

(14) Casiano-Negroni, A., Sun, X., and Al-Hashimi, H. M. (2007) Probing Na(+)-induced changes in the HIV-1 TAR conformational dynamics using NMR residual dipolar couplings: New insights into the role of counterions and electrostatic interactions in adaptive recognition. *Biochemistry 46*, 6525−6535.

(15) Fedor, M. J. (2002) The role of metal ions in RNA catalysis. *Curr. Opin. Struct. Biol. 12*, 289−295.

(16) Sigel, R. K., and Pyle, A. M. (2007) Alternative roles for metal ions in enzyme catalysis and the implications for ribozyme chemistry. *Chem. Rev. 107*, 97−113.

(17) Chen, J., Ganguly, A., Miswan, Z., Hammes-Schiffer, S., Bevilacqua, P. C., and Golden, B. L. (2013) Identification of the catalytic Mg^{2+} ion in the hepatitis delta virus ribozyme. *Biochemistry 52*, 557−567.

(18) Gordon, P. M., Fong, R., and Piccirilli, J. A. (2007) A second divalent metal ion in the group II intron reaction center. *Chem. Biol. 14*, 607−612.

(19) Thaplyal, P., Ganguly, A., Golden, B. L., Hammes-Schiffer, S., and Bevilacqua, P. C. (2013) Thio effects and an unconventional metal ion rescue in the genomic hepatitis delta virus ribozyme. *Biochemistry 52*, 6499−6514.

(20) Lonnberg, T., and Lonnberg, H. (2005) Chemical models for ribozyme action. *Curr. Opin. Chem. Biol. 9*, 665−673.

(21) Herschlag, D., and Jencks, W. P. (1990) Catalysis of the hydrolysis of phosphorylated pyridines by $Mg(OH)^+$: A possible model for enzymatic phosphoryl transfer. *Biochemistry 29*, 5172−5179.

(22) Narlikar, G. J., Gopalakrishnan, V., McConnell, T. S., Usman, N., and Herschlag, D. (1995) Use of binding energy by an RNA enzyme for catalysis by positioning and substrate destabilization. *Proc. Natl. Acad. Sci. U.S.A. 92*, 3668−3672.

(23) Lippert, B. (2008) Ligand-pKa shifts through metals: Potential relevance to ribozyme chemistry. *Chem. Biodiversity 5*, 1455−1474.
(24) Smith, M. D., Mehdizadeh, R., Olive, J. E., and Collins, R. A. (2008) The ionic environment determines ribozyme cleavage rate by modulation of nucleobase pKa. *RNA 14*, 1942−1949.
(25) Saville, B. J., and Collins, R. A. (1990) A site-specific self-cleavage reaction performed by a novel RNA in *Neurospora* mitochondria. *Cell 61*, 685−696.
(26) Collins, R. A. (2002) The *Neurospora* Varkud satellite ribozyme. *Biochem. Soc. Trans. 30*, 1122−1126.
(27) Lilley, D. M. (2004) The Varkud satellite ribozyme. *RNA 10*, 151−158.
(28) Lilley, D. M. J. (2008) The hairpin and Varkud satellite ribozymes, In *Ribozymes and RNA Catalysis* (Lilley, D. M. J., and Eckstein, F., Eds.), pp 66−91, RSC Publishing, Cambridge, UK.
(29) Cochrane, J. C., and Strobel, S. A. (2008) Catalytic strategies of self-cleaving ribozymes. *Acc. Chem. Res. 41*, 1027−1035.
(30) Wilson, T. J., and Lilley, D. M. (2011) Do the hairpin and VS ribozymes share a common catalytic mechanism based on general acid-base catalysis? A critical assessment of available experimental data. *RNA 17*, 213−221.
(31) Beattie, T. L., Olive, J. E., and Collins, R. A. (1995) A secondary-structure model for the self-cleaving region of *Neurospora* VS RNA. *Proc. Natl. Acad. Sci. U.S.A. 92*, 4686−4690.
(32) Andersen, A., and Collins, R. A. (2000) Rearrangement of a stable RNA secondary structure during VS ribozyme catalysis. *Mol. Cell 5*, 469−478.
(33) Andersen, A. A., and Collins, R. A. (2001) Intramolecular secondary structure rearrangement by the kissing interaction of the *Neurospora* VS ribozyme. *Proc. Natl. Acad. Sci U.S.A. 98*, 7730−7735.
(34) Bouchard, P., and Legault, P. (2013) Structural insights into substrate recognition by the *Neurospora* Varkud satellite ribozyme: Importance of U-turns at the kissing-loop junction. *Biochemistry* [Online early access]. DOI: 10.1021/bi401491g. Published Online: Dec 10, 2013.
(35) Hiley, S. L., and Collins, R. A. (2001) Rapid formation of a solvent-inaccessible core in the *Neurospora* Varkud satellite ribozyme. *EMBO J. 20*, 5461−5469.
(36) Lafontaine, D. A., Wilson, T. J., Norman, D. G., and Lilley, D. M. (2001) The A730 loop is an important component of the active site of the VS ribozyme. *J. Mol. Biol. 312*, 663−674.
(37) Hiley, S. L., Sood, V. D., Fan, J., and Collins, R. A. (2002) 4-Thio-U cross-linking identifies the active site of the VS ribozyme. *EMBO J. 21*, 4691−4698.
(38) Lafontaine, D. A., Wilson, T. J., Zhao, Z.-Y., and Lilley, D. M. J. (2002) Functional group requirements in the probable active site of the VS ribozyme. *J. Mol. Biol. 323*, 23−34.
(39) Sood, V. D., and Collins, R. A. (2002) Identification of the catalytic subdomain of the VS ribozyme and evidence for remarkable sequence tolerance in the active site loop. *J. Mol. Biol. 320*, 443−454.
(40) Jones, F. D., and Strobel, S. A. (2003) Ionization of a critical adenosine residue in the *Neurospora* Varkud satellite ribozyme active site. *Biochemistry 42*, 4265−4276.
(41) McLeod, A. C., and Lilley, D. M. (2004) Efficient, pH-dependent RNA ligation by the VS ribozyme in trans. *Biochemistry 43*, 1118−1125.
(42) Zhao, Z. Y., McLeod, A., Harusawa, S., Araki, L., Yamaguchi, M., Kurihara, T., and Lilley, D. M. (2005) Nucleobase participation in ribozyme catalysis. *J. Am. Chem. Soc. 127*, 5026−5027.
(43) Smith, M. D., and Collins, R. A. (2007) Evidence for proton transfer in the rate-limiting step of a fast-cleaving Varkud satellite ribozyme. *Proc. Natl. Acad. Sci. U.S.A. 104*, 5818−5823.
(44) Wilson, T. J., McLeod, A. C., and Lilley, D. M. (2007) A guanine nucleobase important for catalysis by the VS ribozyme. *EMBO J. 26*, 2489−2500.
(45) Jaikaran, D., Smith, M. D., Mehdizadeh, R., Olive, J., and Collins, R. A. (2008) An important role of G638 in the cis-cleavage reaction of the *Neurospora* VS ribozyme revealed by a novel nucleotide analog incorporation method. *RNA 14*, 938−949.
(46) Wilson, T. J., Li, N. S., Lu, J., Frederiksen, J. K., Piccirilli, J. A., and Lilley, D. M. (2010) Nucleobase-mediated general acid-base catalysis in the Varkud satellite ribozyme. *Proc. Natl. Acad. Sci. U.S.A 107*, 11751−11756.
(47) Collins, R. A., and Olive, J. E. (1993) Reaction conditions and kinetics of self-cleavage of a ribozyme derived from *Neurospora* VS RNA. *Biochemistry 32*, 2795−2799.
(48) Murray, J. B., Seyhan, A. A., Walter, N. G., Burke, J. M., and Scott, W. G. (1998) The hammerhead, hairpin and VS ribozymes are catalytically proficient in monovalent cations alone. *Chem. Biol. 5*, 587−595.
(49) Lafontaine, D. A., Norman, D. G., and Lilley, D. M. (2001) Structure, folding and activity of the VS ribozyme: Importance of the 2-3-6 helical junction. *EMBO J. 20*, 1415−1424.
(50) Desjardins, G., Bonneau, E., Girard, N., Boisbouvier, J., and Legault, P. (2011) NMR structure of the A730 loop of the *Neurospora* VS ribozyme: Insights into the formation of the active site. *Nucleic Acids Res. 39*, 4427−4437.
(51) Sood, V. D., Beattie, T. L., and Collins, R. A. (1998) Identification of phosphate groups involved in metal binding and tertiary interactions in the core of the *Neurospora* VS ribozyme. *J. Mol. Biol. 282*, 741−750.
(52) Tzokov, S. B., Murray, I. A., and Grasby, J. A. (2002) The role of magnesium ions and 2′-hydroxyl groups in the VS ribozyme-substrate interaction. *J. Mol. Biol. 324*, 215−226.
(53) Hoffmann, B., Mitchell, G. T., Gendron, P., Major, F., Andersen, A. A., Collins, R. A., and Legault, P. (2003) NMR structure of the active conformation of the Varkud satellite ribozyme cleavage site. *Proc. Natl. Acad. Sci. U.S.A. 100*, 7003−7008.
(54) Kovacheva, Y. S., Tzokov, S. B., Murray, I. A., and Grasby, J. A. (2004) The role of phosphate groups in the VS ribozyme-substrate interaction. *Nucleic Acids Res. 32*, 6240−6250.
(55) Campbell, D. O., and Legault, P. (2005) NMR structure of the Varkud satellite ribozyme stem-loop V RNA and magnesium-ion binding from chemical-shift mapping. *Biochemistry 44*, 4157−4170.
(56) Slim, G., and Gait, M. J. (1991) Configurationally defined phosphorothioate-containing oligoribonucleotides in the study of the mechanism of cleavage of hammerhead ribozymes. *Nucleic Acids Res. 19*, 1183−1188.
(57) Delaglio, F., Grzesiek, S., Vuister, G. W., Zhu, G., Pfeifer, J., and Bax, A. (1995) NMRPipe: A multidimensional spectral processing system based on UNIX pipes. *J. Biomol. NMR 6*, 277−293.
(58) Johnson, B. A., and Blevins, R. A. (1994) NMRView: A computer program for the visualization and analysis of NMR data. *J. Biomol. NMR 4*, 603−614.
(59) Wishart, D. S., Bigam, C. G., Yao, J., Dyson, H. J., Oldfield, E., Markley, J. L., and Sykes, B. D. (1995) ^{1}H, ^{13}C, ^{15}N chemical shift referencing in biomolecular NMR. *J. Biomol. NMR 6*, 135−140.
(60) Vuister, G. W., and Bax, A. (1992) Resolution enhancement and spectral editing of uniformly ^{13}C-enriched proteins by homonuclear broadband ^{13}C decoupling. *J. Magn. Reson. 98*, 428−435.
(61) Santoro, J., and King, G. C. (1992) A constant-time 2D overbodenhausen experiment for inverse correlation of isotopically enriched species. *J. Magn. Reson. 97*, 202−207.
(62) Ikura, M., Kay, L. E., Tschudin, R., and Bax, A. (1990) Three-dimensional NOESY-HMQC spectroscopy of a ^{13}C-labeled protein. *J. Magn. Reson. 86*, 204−209.
(63) Piotto, M., Saudek, V., and Skleñár, V. (1992) Gradient-tailored excitation for single-quantum NMR spectroscopy of aqueous solutions. *J. Biomol. NMR 2*, 661−665.
(64) Kay, L. E., Keifer, P., and Saarinen, T. (1992) Pure absorption gradient enhanced heteronuclear single quantum correlation spectroscopy with improved sensitivity. *J. Am. Chem. Soc. 114*, 10663−10665.
(65) Skleñár, V., Peterson, R. D., Rejante, M. R., and Feigon, J. (1994) Correlation of nucleotide base and sugar protons in a ^{15}N-labeled HIV-1 RNA oligonucleotide by ^{1}H−^{15}N HSQC experiments. *J. Biomol. NMR 4*, 117−122.

(66) Schwieters, C. D., Kuszewski, J. J., Tjandra, N., and Clore, G. M. (2003) The Xplor-NIH NMR molecular structure determination package. *J. Magn. Reson. 160*, 66−74.
(67) Kleywegt, G. T., and Jones, T. A. (1998) Databases in protein crystallography. *Acta Crystallogr., Sect. D 54*, 1119−11131.
(68) Petrov, A. I., Zirbel, C. L., and Leontis, N. B. (2011) WebFR3D−a server for finding, aligning and analyzing recurrent RNA 3D motifs. *Nucleic Acids Res. 39*, W50−55.
(69) Bertini, I., and Lychinat, C. (1986) *NMR of Paramagnetic Molecules in Biological Systems*, Benjamin/Cummings, Menlo Park, CA.
(70) Ott, G., Arnold, L., and Limmer, S. (1993) Proton NMR studies of manganese ion binding to tRNA-derived acceptor arm duplexes. *Nucleic Acids Res. 21*, 5859−5864.
(71) Allain, F. H., and Varani, G. (1995) Divalent metal ion binding to a conserved wobble pair defining the upstream site of cleavage of group I self-splicing introns. *Nucleic Acids Res. 23*, 341−350.
(72) Hansen, M. R., Simorre, J. P., Hanson, P. P., Mokler, V., Bellon, L., Beigelman, L., and Pardi, A. (1999) Identification and characterization of a novel high affinity metal-binding site in the hammerhead ribozyme. *RNA 5*, 1099−1104.
(73) Colmenarejo, G., and Tinoco, I., Jr. (1999) Structure and thermodynamics of metal binding in the P5 helix of a group I intron ribozyme. *J. Mol. Biol. 290*, 119−135.
(74) Butcher, S. E., Allain, F. H.-T., and Feigon, J. (2000) Determination of metal ion binding sites within the hairpin ribozyme domains by NMR. *Biochemistry 39*, 2174−2182.
(75) Zuleeg, T., Hartmann, R. K., Kreutzer, R., and Limmer, S. (2001) NMR spectroscopic evidence for Mn(2+)(Mg(2+)) binding to a precursor-tRNA microhelix near the potential RNase P cleavage site. *J. Mol. Biol. 305*, 181−189.
(76) Davis, J. H., Foster, T. R., Tonelli, M., and Butcher, S. E. (2007) Role of metal ions in the tetraloop-receptor complex as analyzed by NMR. *RNA 13*, 76−86.
(77) Granot, J., Feigon, J., and Kearns, D. R. (1982) Interactions of DNA with divalent ions. I. ^{31}P-NMR studies. *Biopolymers 21*, 181−201.
(78) Bertini, I., Luchinat, C., and Scozzafava, A. (1978) A ^{31}P NMR study of phosphate in presence of cobalt(II)- and copper(II)-substituted bovine carbonic anhydrase B. *FEBS Lett. 93*, 251−254.
(79) Maderia, M., Horton, T. E., and DeRose, V. J. (2000) Metal interactions with a GAAA RNA tetraloop characterized by ^{31}P NMR and phosphorothioate substitution. *Biochemistry 39*, 8193−8200.
(80) Maderia, M., Hunsicker, L. M., and DeRose, V. J. (2000) Metal-phosphate interactions in the hammerhead ribozyme observed by ^{31}P NMR and phosphorothioate substitutions. *Biochemistry 39*, 12113−12120.
(81) Duguid, J. G., and Bloomfield, V. A. (1995) Aggregation of melted DNA by divalent metal ion-mediated cross-linking. *Biophys. J. 69*, 2642−2648.
(82) Duguid, J. G., Bloomfield, V. A., Benevides, J. M., and Thomas, G. J., Jr. (1995) Raman spectroscopy of DNA-metal complexes. II. The thermal denaturation of DNA in the presence of Sr^{2+}, Ba^{2+}, Mg^{2+}, Ca^{2+}, Mn^{2+}, Co^{2+}, Ni^{2+}, and Cd^{2+}. *Biophys. J. 69*, 2623−2641.
(83) Horton, T. E., Maderia, M., and DeRose, V. J. (2000) Impact of phosphorothioate substitutions on the thermodynamic stability of an RNA GAAA tetraloop: An unexpected stabilization. *Biochemistry 39*, 8201−8207.
(84) Smith, J. S., and Nikonowicz, E. P. (2000) Phosphorothioate substitution can substantially alter RNA conformation. *Biochemistry 39*, 5642−5652.
(85) McFail-Isom, L., Shui, X., and Williams, L. D. (1998) Divalent cations stabilize unstacked conformations of DNA and RNA by interacting with base pi systems. *Biochemistry 37*, 17105−17111.
(86) Huppler, A., Niksstad, L. J., Allman, A. M., Brow, D. A., and Butcher, S. E. (2002) Metal binding and base ionization in the U6 RNA intramolecular stem-loop structure. *Nat. Struct. Biol. 9*, 431−435.
(87) Osborne, E. M., Ward, W. L., Ruehle, M. Z., and DeRose, V. J. (2009) The identity of the nucleophile substitution may influence metal interactions with the cleavage site of the minimal hammerhead ribozyme. *Biochemistry 48*, 10654−10664.
(88) Ward, W. L., and Derose, V. J. (2012) Ground-state coordination of a catalytic metal to the scissile phosphate of a tertiary-stabilized Hammerhead ribozyme. *RNA 18*, 16−23.
(89) Ennifar, E., Walter, P., and Dumas, P. (2003) A crystallographic study of the binding of 13 metal ions to two related RNA duplexes. *Nucleic Acids Res. 31*, 2671−2682.
(90) Kieft, J. S., and Tinoco, I. J. (1997) Solution structure of a metal-binding site in the major groove of RNA complexed with cobalt(III) hexammine. *Curr. Biol. 5*, 713−721.
(91) Keel, A. Y., Rambo, R. P., Batey, R. T., and Kieft, J. S. (2007) A general strategy to solve the phase problem in RNA crystallography. *Structure 15*, 761−772.
(92) Chen, J. H., Gong, B., Bevilacqua, P. C., Carey, P. R., and Golden, B. L. (2009) A catalytic metal ion interacts with the cleavage Site G.U wobble in the HDV ribozyme. *Biochemistry 48*, 1498−1507.
(93) Chen, J. H., Yajima, R., Chadalavada, D. M., Chase, E., Bevilacqua, P. C., and Golden, B. L. (2010) A 1.9 Å crystal structure of the HDV ribozyme precleavage suggests both Lewis acid and general acid mechanisms contribute to phosphodiester cleavage. *Biochemistry 49*, 6508−6518.
(94) Carter, A. P., Clemons, W. M., Jr., Brodersen, D. E., Wimberley, B. T., Morgan-Warren, R., and Ramakrishnan, V. (2000) Functional insights from the structure of the 30S ribosomal subunit and its interactions with antibiotics. *Nature 407*, 340−348.
(95) Rüdisser, S., and Tinoco, I. J. (2000) Solution structure of cobalt(III) hexammine complexed to the GAAA tetraloop, and metal-ion binding to G-A mismatches. *J. Mol. Biol. 295*, 1211−1223.
(96) Mundoma, C., and Greenbaum, N. L. (2002) Sequestering of Eu(III) by a GAAA RNA tetraloop. *J. Am. Chem. Soc. 124*, 3525−3532.
(97) Seetharaman, M., Eldho, N. V., Padgett, R. A., and Dayie, K. T. (2006) Structure of a self-splicing group II intron catalytic effector domain 5: Parallels with spliceosomal U6 RNA. *RNA 12*, 235−247.
(98) Szewczak, A. A., Moore, P. B., Chang, Y. L., and Wool, I. G. (1993) The conformation of the sarcin/ricin loop from 28S ribosomal RNA. *Proc. Natl. Acad. Sci. U.S.A. 90*, 9581−9585.
(99) Wimberly, B., Varani, G., and Tinoco, I., Jr. (1993) The conformation of loop E of eukaryotic 5S ribosomal RNA. *Biochemistry 32*, 1078−1087.
(100) Correll, C. C., Munishkin, A., Chan, Y. L., Ren, Z., Wool, I. G., and Steitz, T. A. (1998) Crystal structure of the ribosomal RNA domain essential for binding elongation factors. *Proc. Natl. Acad. Sci. U.S.A. 95*, 13436−13441.
(101) Butcher, S. E., Allain, F. H., and Feigon, J. (1999) Solution structure of the loop B domain from the hairpin ribozyme. *Nat. Struct. Biol. 6*, 212−216.
(102) Zimmermann, G. R., Wick, C. L., Shields, T. P., Jenison, R. D., and Pardi, A. (2000) Molecular interactions and metal binding in the theophylline-binding core of an RNA aptamer. *RNA 6*, 659−667.
(103) Rupert, P. B., and Ferré-D'Amaré, A. R. (2001) Crystal structure of a haripin ribozyme-inhibitor complex with implications for catalysis. *Nature 410*, 780−786.
(104) Alam, S., Grum-Tokars, V., Krucinska, J., Kundracik, M. L., and Wedekind, J. E. (2005) Conformational heterogeneity at position U37 of an all-RNA hairpin ribozyme with implications for metal binding and the catalytic structure of the S-turn. *Biochemistry 44*, 14396−14408.